International Journal of Thermal Sciences 48 (2009) 1477–1485

Contents lists available at ScienceDirect

International Journal of Thermal Sciences

www.elsevier.com/locate/ijts

An axisymmetric dual-phase-lag bioheat model for laser heating of living tissues

Jianhua Zhou, Yuwen Zhang *, J.K. Chen

Department of Mechanical and Aerospace Engineering, University of Missouri, Columbia, MO 65211, USA

ARTICLE INFO

Article history:
Received 8 August 2008
Received in revised form 25 November 2008
Accepted 5 December 2008
Available online 14 January 2009

Keywords:
Laser
Bioheat transfer
Living tissue

ABSTRACT

A two-dimensional (2D) axisymmetric dual-phase-lag (DPL) model is proposed to describe heat transfer in living biological tissues with nonhomogeneous inner structures. The DPL constitutive equation is incorporated, for the first time, into the 2D axisymmetric bioheat transfer model in living tissues, and corresponding numerical approach is developed. Two heating schemes (surface heating and body heating) and two beam profiles (flat beam and Gaussian beam) are examined in detail. The numerical results indicate that the DPL bioheat conduction model describes different thermal responses from the thermal-wave and Pennes' bioheat conduction models, depending on the values of the two lagging times. For a local heating with the heated spot smaller than the tissue bulk, the variations of the non-uniform distributions of temperature suggest that the multi-dimensional effects of thermal wave and diffusion not be negligible. It is also found that due to the presence of blood perfusion in living tissues, the present DPL bioheat conduction model reduces to the Pennes' bioheat model only when $\tau_q = \tau_T = 0$.

1. Introduction

For the past several decades, temperature predictions for biological bodies have attracted great attentions due to its significance in clinical, basic, aeronautic, environmental sciences, etc. Most analyses are based on the well-known Pennes' bioheat equation [1]:

$$\rho c\frac{\partial T}{\partial t} = \nabla\cdot(k\nabla T) + w_b\rho_b c_b(T_b - T) + Q_m + Q \tag{1}$$

The heat conduction term in the Pennes' bioheat equation (1) is based on the classical Fourier's law that implies an infinite thermal propagation speed. To remedy this physically unreasonable deficiency, the Pennes' bioheat equation has been modified by including the thermal wave effects [2–8]:

$$\mathbf{q}(\mathbf{r},t) + \tau\frac{\partial \mathbf{q}(\mathbf{r},t)}{\partial t} = -k\nabla T(\mathbf{r},t) \tag{2}$$

The theoretical value of thermal relaxation time τ in biological systems was predicted to be 20–30 s [3], and a value of approximately 16 s was experimentally observed [4]. Although the non-Fourier thermal wave model [2–8] can solve the paradox of infinite thermal propagation speed, it cannot capture the microscale response in space [9] and may introduce some unusual behaviors and physically impossible solutions such as negative thermal energies [10,11].

More recently, Antaki [12] has employed the dual-phase-lag (DPL) heat conduction model, which is based on the well-known two phase lags concept [13], to interpret the non-Fourier heat conduction phenomena in processed meats:

$$\mathbf{q}(\mathbf{r},t) + \tau_q\frac{\partial \mathbf{q}(\mathbf{r},t)}{\partial t} = -k\left\{\nabla T(\mathbf{r},t) + \tau_T\frac{\partial}{\partial t}\left[\nabla T(\mathbf{r},t)\right]\right\} \tag{3}$$

where τ_T is the phase lag time for temperature gradient, and τ_q is the phase lag time for heat flux. He showed that the DPL heat conduction model correlates better with experimental data, compared to the hyperbolic thermal wave and Fourier heat conduction models.

Eq. (3) shows that the temperature gradient established across a tissue volume located at a position $\mathbf{r}$ at time $t + \tau_T$ results in a heat flux to flow at a different instant of time $t + \tau_q$. For biological tissues, τ_T represents a measure of the time delay in conduction that occurs along microscopic paths (e.g., within meat particles) and τ_q is a measure of the time delay in conduction (e.g., contact resistance between different tissue constituents) [12]. Eq. (3) reduces to Eq. (2) when $\tau_T = 0$ and to the classical Fourier law by further letting $\tau_q = 0$.

Currently, there exists a lot of controversy in the literature about whether or not DPL conduction and, more generally, any non-Fourier conduction is important for biological tissues. Specifically, there is limited experimental evidence for this phenomenon, and some of the non-Fourier evidence has been called into question repeatedly. An excellent review on this topic can be found in [14].

Although the validity of various non-Fourier models is debatable, no ultimate conclusion has been drawn at present due to the

* Corresponding author.
E-mail address: ZhangYu@missouri.edu (Y. Zhang).

1290-0729/$ – see front matter
doi:10.1016/j.ijthermalsci.2008.12.012

Nomenclature

c_b	specific heat of blood	J/(kg K)
c	specific heat of tissues	J/(kg K)
k	thermal conductivity of tissue	W/(m K)
L_x	total number of grid points in x-direction	
M_r	total number of grid points in r-direction	
q_p	incident heat flux	W/m^2
$\mathbf{q}$	heat flux vector	W/m^2
$q_{p\max}$	peak value at the spot center for a Gaussian-type heating flux case	W/m^2
q_r	heat flux component in r-direction	W/m^2
q_x	heat flux component in x-direction	W/m^2
Q	heat source due to other reasons	W/m^3
Q_m	metabolic heat generation	W/m^3
$\mathbf{r}$	coordinate variable in radial direction	m
r_o	radius of the tissue cylinder	m
r_p	radius of the heating spot	m
r	position vector	m
t	time	s
t_p	duration time of the heating process	s
T	tissue temperature	K
T_o	initial tissue temperature	K
T_b	blood temperature	K
w_b	blood perfusion rate	m^3/(m^3 tissue s)
x	coordinate variable in axial direction	m
x_o	thickness of the cylinder tissue	m

Greek symbols

α	thermal diffusivity	m^2/s
δx	distance between two neighboring grid points in x-direction	m
δr	distance between two neighboring grid points in r-direction	m
μ_a	absorption coefficient	m^{-1}
ρ	tissue mass density	kg/m^3
ρ_b	blood mass density	kg/m^3
τ	thermal relaxation time in hyperbolic model	s
τ_q	phase lag of the heat flux	s
τ_T	phase lag of the temperature gradient	s
Δr	size of each control volume in r-direction	m
Δt	time step	s
Δx	size of each control volume in x-direction	m

complexity of biological systems. Recently, some physical anomalies concerning the DPL model have been reported for several particular cases [15]. Nevertheless, because the dual-phase-lag model offers the possibility to conveniently capture—at macroscale level—some microscale processes of conduction, it has attracted a great deal of attention over the last ten years. The authors recently developed a one-dimensional DPL bioheat transfer model to investigate the thermal response of living biological tissues to laser irradiation [16]. Xu et al. [17] derived the bioheat equation in the vector format and used the derived equation to study the 1D thermal damage of skin. The 1D approximation is adequate only for the cases where thermal loads are uniform over the heated spot area and the spot size is much larger than the thermal characteristic length of the media. For other cases, multi-dimensional thermal transport effects may not be negligible. In this study, numerical solution based on the 2D axisymmetric assumption for living tissues under a surface laser heating and a body laser heating are carried out. The transient and spatial temperature profiles are compared for different phase lag times, including the special cases of thermal wave and Pennes' bioheat conduction models.

2. DPL bioheat model formulation

The bioheat energy balance equation considering blood perfusion and metabolic heat generation is given by [1]:

$$\rho c\frac{\partial T}{\partial t} = -\nabla\cdot\mathbf{q} + w_b\rho_b c_b(T_b - T) + Q_m + Q \tag{4}$$

The specific forms of bioheat conduction equation depend upon the constitutive relation between the heat flux $\mathbf{q}$ and temperature T.

Combining the energy balance equation (4) and the dual-phase-lag constitutive relation (3) while eliminating the heat flux $\mathbf{q}$ leads to the following DPL bioheat conduction equation for tissue temperature:

$$\tau_q\frac{\partial^2 T}{\partial t^2} + \left(1 + \frac{w_b\rho_b c_b}{\rho c}\tau_q\right)\frac{\partial T}{\partial t} = \alpha\nabla\cdot(\nabla T) + \alpha\tau_T\frac{\partial}{\partial t}\left[\nabla\cdot(\nabla T)\right] + \frac{w_b\rho_b c_b}{\rho c}(T_b - T) + \frac{w_b\rho_b c_b\tau_q}{\rho c}\frac{\partial T_b}{\partial t} + \frac{Q_m + Q}{\rho c} + \frac{\tau_q}{\rho c}\left(\frac{\partial Q_m}{\partial t} + \frac{\partial Q}{\partial t}\right) \tag{5}$$

The DPL bioheat conduction equation can also be derived for heat flux $\mathbf{q}(\mathbf{r}, t)$ by eliminating the temperature T:

$$\begin{aligned}\frac{\partial\mathbf{q}}{\partial t} + \tau_q\frac{\partial^2\mathbf{q}}{\partial t^2} &= \alpha\nabla(\nabla\bullet\mathbf{q}) + \alpha\tau_T\frac{\partial}{\partial t}\left[\nabla(\nabla\bullet\mathbf{q})\right] \\ &\quad + \alpha w_b\rho_b c_b(\nabla T - \nabla T_b) \\ &\quad + \alpha\tau_T w_b\rho_b c_b\frac{\partial}{\partial t}(\nabla T - \nabla T_b) - \alpha(\nabla Q_m + \nabla Q) \\ &\quad - \alpha\tau_T\left[\frac{\partial}{\partial t}(\nabla Q_m + \nabla Q)\right]\end{aligned} \tag{6}$$

In the derivations of Eqs. (5) and (6), all the thermal properties are assumed to be constant. Each of Eqs. (5) and (6) has more terms compared to their counterpart DPL heat conduction equation for industry materials. Attention is paid to those terms involving the blood perfusion with tissue temperature T. There is no coupling between T and $\mathbf{q}$ in the temperature formulation (5), whereas the coupling exists in the heat flux formulation (6).

For numerical analysis, we consider a cylindrical biological tissue of radius r_o and thickness x_o irradiated by electromagnetic waves normally to the upper surface ($x = 0$) over a circular spot of radius r_p for a time period t_p (Fig. 1). The living tissue is initially at a uniform temperature T_o. Assume that the irradiation is uniform or in a Gaussian distribution. The thermal load can be modeled as a surface heat flux or a body heat source, depending on the irradiation penetration depth. Let the center of the incident heat flux $q_p(r)$ coincide with the origin O of the cylindrical coordinate system. The other boundary surfaces are assumed to be thermally insulated. Due to the axisymmetry of the tissue geometry and the thermal load, only a 2D axisymmetric cylindrical domain *OABC* (Fig. 1) needs to be analyzed for the thermal transfer in the tissue.

In this study, the heat flux formulation of the DPL bioheat conduction, i.e., Eq. (6), is adopted for analyzing the heat conduction in the living tissue shown in Fig. 1 since it is more convenient for problems involving only heat flux boundary conditions. Although blood temperature T_b and the metabolic heat generation Q_m may vary with time and space, they are assumed to be constant here for

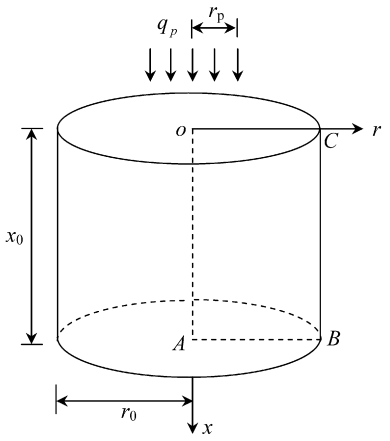

Fig. 1. A schematic model of a cylindrical tissue and coordinate system subjected to an incident heat flux.

emphasizing the essential physics of the DPL bioheat transfer. Under this assumption, those terms with the gradients of T_b and Q_m can be dropped off from Eq. (6). Accordingly, the two axisymmetric equations governing the heat transfers in the r- and x-direction can be expressed from Eq. (6):

$$\frac{\partial q_r}{\partial t}+\tau_q\frac{\partial^2 q_r}{\partial t^2}=\alpha\frac{\partial}{\partial r}\left\{\frac{1}{r}\left[\frac{\partial(rq_r)}{\partial r}+\frac{\partial(rq_x)}{\partial x}\right]\right\}+\alpha\tau_T\frac{\partial^2}{\partial r\partial t}\left\{\frac{1}{r}\left[\frac{\partial(rq_r)}{\partial r}+\frac{\partial(rq_x)}{\partial x}\right]\right\}+\alpha w_b\rho_b c_b\frac{\partial T}{\partial r}+\alpha w_b\rho_b c_b\tau_T\frac{\partial^2 T}{\partial r\partial t}-\alpha\frac{\partial Q}{\partial r}-\alpha\tau_T\frac{\partial^2 Q}{\partial r\partial t} \tag{7}$$

$$\frac{\partial q_x}{\partial t}+\tau_q\frac{\partial^2 q_x}{\partial t^2}=\alpha\frac{\partial}{\partial x}\left\{\frac{1}{r}\left[\frac{\partial(rq_r)}{\partial r}+\frac{\partial(rq_x)}{\partial x}\right]\right\}+\alpha\tau_T\frac{\partial^2}{\partial x\partial t}\left\{\frac{1}{r}\left[\frac{\partial(rq_r)}{\partial r}+\frac{\partial(rq_x)}{\partial x}\right]\right\}+\alpha w_b\rho_b c_b\frac{\partial T}{\partial x}+\alpha w_b\rho_b c_b\tau_T\frac{\partial^2 T}{\partial x\partial t}-\alpha\frac{\partial Q}{\partial x}-\alpha\tau_T\frac{\partial^2 Q}{\partial x\partial t} \tag{8}$$

Eqs. (7) and (8) will be solved with proper initial and boundary conditions. In this study, the initial conditions of the heat flux and its time-rate are assumed to be zero,

$$q_r=q_x=0,\qquad \frac{\partial q_r}{\partial t}=\frac{\partial q_x}{\partial t}=0 \quad \text{for } 0\leqslant r\leqslant r_o \text{ and } 0\leqslant x\leqslant x_o \quad \text{when } t=0 \tag{9}$$

The boundary conditions are given by:

$$\begin{aligned}
&q_x=q_p(r) && \text{for } 0\leqslant r\leqslant r_p \text{ and } x=0 && \text{when } 0<t\leqslant t_p\\
&q_x=0 && \text{for } r_p<r\leqslant r_o \text{ and } x=0 && \text{when } t>t_p\\
&q_x=0 && \text{for } 0\leqslant r\leqslant r_o \text{ and } x=x_o && \text{when } t>0\\
&q_r=0 && \text{for } 0\leqslant x\leqslant x_o \text{ and } r=0 && \text{when } t>0\\
&q_r=0 && \text{for } 0\leqslant x\leqslant x_o \text{ and } r=r_o && \text{when } t>0
\end{aligned} \tag{10}$$

The first equation of Eq. (10) is for the case of surface heating. It is changed to

$$q_x=0 \quad \text{for } 0\leqslant r\leqslant r_p \text{ and } x=0 \quad \text{when } 0<t\leqslant t_p \tag{11}$$

when a body heating is considered.

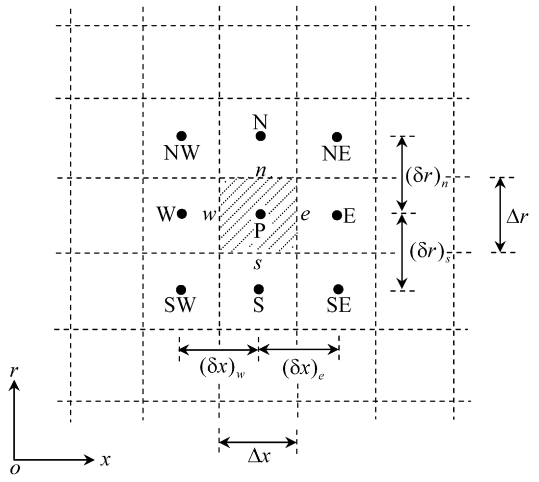

Fig. 2. Control volumes and grid points for a 2D axisymmetric domain.

The control volume method [18] is employed to solve the governing equations (7) and (8) together with the initial and boundary conditions (9)–(11). The derivation of the discretizing equations and numerical algorithm are given in Appendix A.

3. Validation of computer code

The solution of the 2D axisymmetric DPL numerical model is first validated with a test problem. The simulation model is the same as that shown in Fig. 1. The difference is that the upper surface of the cylinder is subject to a first kind of boundary condition rather than laser heating. To keep consistency with the analytical solution presented in [13], the numerical simulation is performed based on dimensionless quantities. The thickness and the radius of the cylinder are $x_0=1$ and $r_0=2$, respectively. Initially, the cylinder is uniformly at the temperature of $T_0=0$. From time $t>0$, the temperature of a finite circular area (whose center is located at $(0,0)$) at the upper surface of the cylinder is elevated to $T_b=1$. The radius of the finite heating area is denoted by r_p, which changes from 0.05 to 1.0. Other boundaries of the cylinder remain at zero temperature gradient. The temperature formulation of the 2D DPL model (i.e., Eq. (5)) will be used to simulate this test problem. The blood perfusion and metabolic heat generation are turned off in order to make our numerical simulation results comparable with analytical solution [13]. Other simulation parameters (which are also non-dimensional) are as follows: thermal diffusivity $\alpha=1$, phase lag time of heat flux $\tau_q=0.05$, phase lag time of temperature $\tau_T=0.001$.

Fig. 3 shows the spatial distribution of temperature along the cylinder centerline ($r=0$) at time $t=0.05$. It can be clearly seen that the 2D temperature distribution gradually approaches the 1D analytical solution [13] when the heating spot size r_p is increased from 0.05 up to 1.0. When the heating spot size becomes equal to the thickness of the cylinder (i.e., $r_p=1.0$, curve 2 in Fig. 3), the calculating results are almost the same as the analytical solution [13]. This indicates that when the heating spot radius is increased up to the thickness of the cylinder, the 2D DPL heat conduction in the cylinder is close to 1D heat conduction. The calculating results presented in Fig. 3 justify the credibility and reliability of the 2D DPL numerical model developed in this study.

4. Results and discussions

When the tissue temperature is elevated to as high as 100 °C, phase change will take place and the tissue can be vaporized. During this stage, pure heat conduction models may not be able to

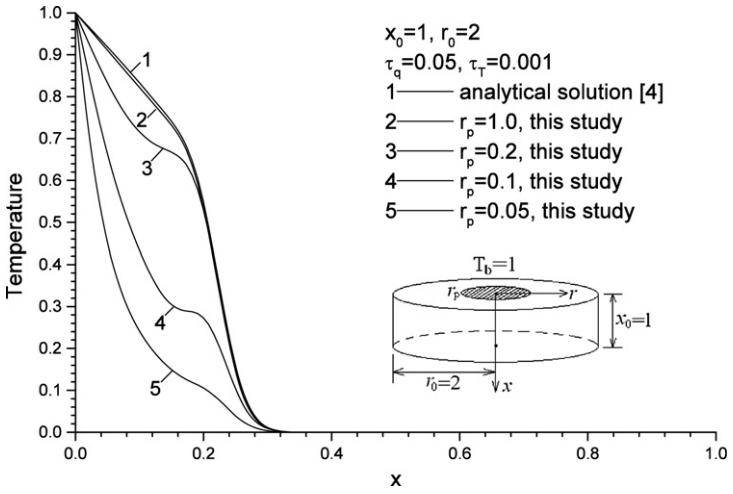

Fig. 3. Verification of the computer code: the 2-D DPL calculating results gradually approach the 1-D analytical solution [13] when the heating spot size r_p is steadily increased Control volumes and grid points for a 2D axisymmetric domain.

describe the complex heat transfer process. The simulation parameters employed in this study are chosen to make sure that the tissue temperature will not exceed 100 °C. The cases studied in this work may find its potential applications in laser hyperthermia or laser coagulation therapy.

Unless otherwise mentioned, the following properties [19] of a biological tissue are used in the following numerical analysis: $\rho = 1000\ \mathrm{kg/m^3}$, $k = 0.628\ \mathrm{W/(m\,K)}$, $c = 4187\ \mathrm{J/(kg\,K)}$ for the thermophysical properties; $\rho_b = 1.06 \times 10^3\ \mathrm{kg/m^3}$, $c_b = 3860\ \mathrm{J/(kg\,K)}$, $w_b = 1.87 \times 10^{-3}\ \mathrm{m^3/(m^3\,tissue\,s)}$, $T_b = 37\,^\circ\mathrm{C}$, $Q_m = 1.19 \times 10^3\ \mathrm{W/m^3}$ for the thermal physical properties and temperature of blood and the metabolic heat generation, respectively. The two phase lag times τ_T and τ_q are ranged from 0.5–32 s. Both the thickness and the radius of the cylindrical tissue are 5 cm, and the initial temperature T_o is 37 °C. The heating lasts for 1 s over a circular spot of radius $r_p = 1$–5 cm.

Convergence study of the grid mesh and time step is first carried out. The two phase lag times τ_T and τ_q are: $\tau_q = 16$ s, $\tau_T = 2$ s. Both the thickness and the radius of the cylindrical tissue are 5 cm, and the initial temperature T_o is 37 °C. The heating lasts for 1 s over a circular spot of radius $r_p = 1$ cm. Fig. 4 shows the transient variations of tissue temperature at the point $(0, 0)$ for different combinations of time step and mesh density. Fig. 4(a) shows the influence of mesh density while time step keeps at $\Delta t = 0.01$ s, and Fig. 4(b) plots the influence of time step while mesh density keeps at $120 * 120$. As can be seen in Fig. 4(a), when the mesh density is increased up to the value $120 * 120$, continuing increase in mesh density cannot result in further improvement of the calculating accuracy. It can be seen in Fig. 4(b) that when the time step is reduced down to the value 0.01 s, more decrease in time step cannot lead to further improvement of the calculating precision. Therefore, a mesh of $120 * 120$ grid points and a time step of 0.01 s are believed to be adequate to give satisfactory results. Thus, they are used in all the simulations in this paper.

Fig. 5 shows the time history of tissue temperature at the point (0, 0) obtained from the present DPL bioheat conduction model for $\tau_q = 16.0$ s and different values of τ_T. In this calculation, the boundary condition of the second kind (the first equation of Eq. (10)) is applied for a surface heating with a constant heat flux $q_p = 4\ \mathrm{W/cm^2}$ and $r_p = 1$ cm. In Fig. 5, the curve 5 is the result obtained from the thermal wave model ($\tau_T = 0$), for which the temperature rise is greatest, followed by several noticeable oscillations. The thermal wave effect is diminished as the lagging time τ_T increases. For clarity, the curves in the time interval 0–5 s are zoomed out in Fig. 5(b). As previously studied [12], the phase lag

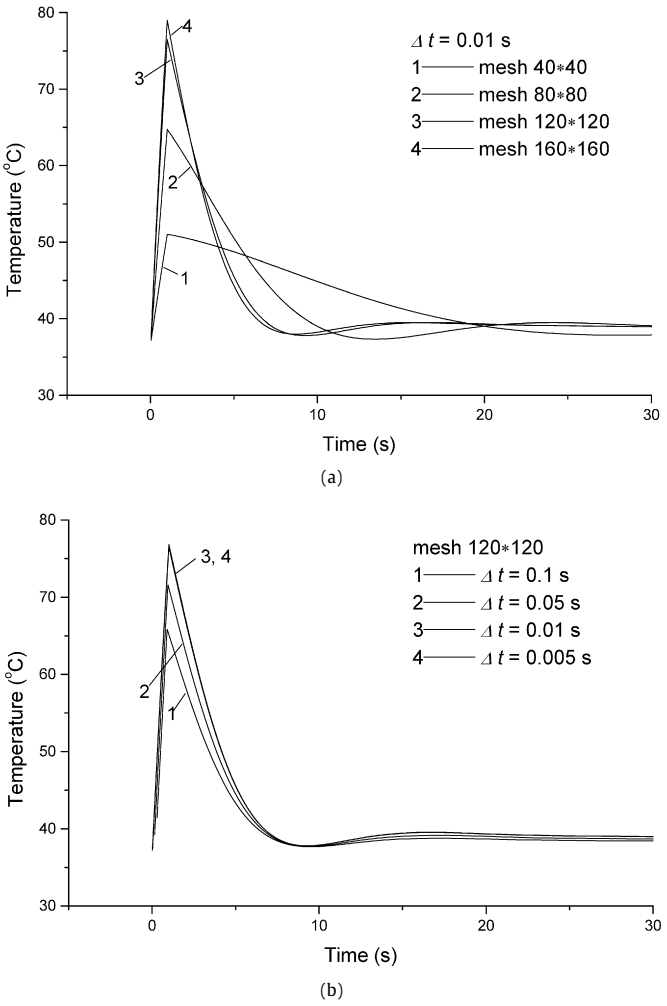

Fig. 4. Convergence study. (a) Influence of mesh density while time step keeps at 0.01 s; (b) Influence of time step while mesh density keeps at $120 * 120$.

τ_T is a measure of the time delay in conduction that occurs along microscopic paths (e.g., within meat particles), which cannot be captured by the classical Fourier approach during nonequilibrium. This delay tends to smooth the sharp wave-fronts by promoting conduction, leading to a non-Fourier diffusion-like conduction. As a result of the phase lag τ_T, the DPL bioheat conduction model

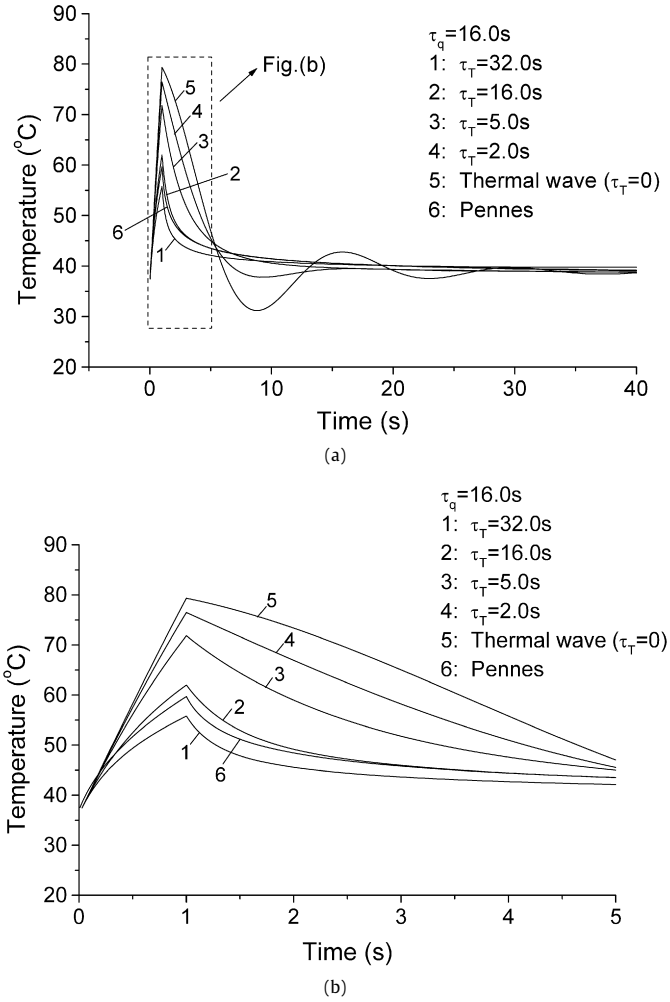

Fig. 5. Temperature transients at point (0, 0) for different τ_T values while τ_q is kept at 16.0 s.

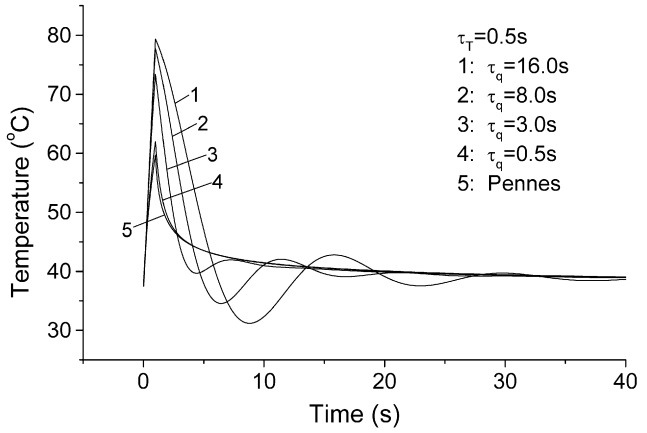

Fig. 6. Temperature transients at point (0, 0) for different τ_q values while τ_T is kept at 0.5 s.

would damp the thermal wave response. When the phase lag τ_T is larger than τ_q, an over-diffusion phenomenon takes place [20], leading to a much lower temperature rise (curve 1 in Fig. 5).

It is interesting to note that the temperature computed with $\tau_q = \tau_T = 16.0$ s (curve 2 in Fig. 5) differs from that computed with the Pennes' bioheat conduction equation ($\tau_q = \tau_T = 0$, curve 6 in Fig. 5). This is in contrast to the traditional DPL heat conduction model for industry materials, for which it approaches the Fourier heat conduction equation when $\tau_q = \tau_T$ (not necessarily equal to zero) [13]. The discrepancy can be attributed to the blood perfusion in the bioheat model. The presence of blood perfusion leads to an extra term involving with τ_q in the temperature formulation (the second term in the parenthesis on the left-hand side of Eq. (5)) and two extra terms involving with τ_T in the heat flux formulation (the fourth and sixth terms on the right-hand side in Eq. (6)). These make the intrinsic characteristic of the DPL bioheat conduction model different from that of the traditional DPL heat conduction model.

Fig. 6 displays the temperature at the point (0, 0) as a function of time for $\tau_T = 0.5$ s and different τ_q. Other parameters used are the same as those in the previous calculation. It is recalled that in biological tissues, the phase lag τ_q represents a measure of the time delay in conduction (e.g., contact resistance between different tissue constituents) during nonequilibrium [12]. This delay tends to induce thermal waves with sharp wave-fronts separating heated and unheated zones in the tissue. The longer the time delay τ_q, the more significant the thermal wave effect. This can be seen from Fig. 6. When τ_q decreases to 0.5 s, the curve of the temperature transient almost overlap with that obtained from the Pennes' bioheat equation, except for the region near the pick temperature (curves 4 and 5 in Fig. 6). It thus is concluded, from the results in Figs. 5 and 6, that the DPL bioheat transfer model would reduce to the Pennes' bioheat conduction model only when $\tau_q = \tau_T = 0$.

Fig. 7 compares the 2D temperature distributions calculated by the DPL and Pennes bioheat conduction models. The phase lag times used here are $\tau_q = 8$ s and $\tau_T = 0.5$ s. The incident heat flux is $q_p = 4$ W/cm^2, and the radius of the heated spot is $r_p = 1$ cm. It can be seen from Figs. 7 (a)–(d) that the thermal wave response, simulated by the DPL bioheat conduction model, occurs in both the axial (Fig. 7(b)) and radial (Figs. 7 (b)–(d)) directions. On the other hand, the classical Pennes' bioheat model leads to smooth temperature distributions (Figs. 7 (e)–(f)). The transients of the tissue temperature, particularly in the region near the heated spot edge, shown in Fig. 7 manifest the inadequacy of the 1D approach.

Fig. 8 shows the transients of temperature at the point (0, 0) for the tissue subjected to a body heating. In this simulation, a uniform irradiation of intensity $q_p = 150$ W/cm^2 is impinging on the top surface $x = 0$ over a circular spot of $r_p = 2$ cm. The volumetric heat source is assumed to follow the Beer's law, $Q(x, r) = \mu_a \cdot q_p \exp(-\mu_a x)$ with the effective absorption coefficient $\mu_a = 1$ cm^{-1}. It can be seen from Fig. 8 that the impact of the phase lags on the temperature response at point (0, 0) is not so pronounced as that found in the case of surface heating (Figs. 5 and 6). The maximum temperature rises are almost the same for all the combinations of the phase lag times τ_T and τ_q studied here. After the irradiation is terminated, the falling rates of the surface temperature are relatively slow, compared to those in Figs. 5 and 6. The 2D temperature distributions at four different time instants are plotted in Fig. 9 for the body heating, simulated with $\tau_q = 8.0$ s and $\tau_T = 0.5$ s. For this body heating with $\mu_a = 1$ cm^{-1}, the resulting temperature distribution in the axial direction is less steep and no thermal wave is found. However, thermal wave does exhibit in the radial direction due to the sharp temperature variation at the heated spot edge (Figs. 9 (c) and (d)).

The foregoing simulations are performed for tissues that are heated by a uniform incident heat flux. In real medical practices, the irradiations can be in Gaussian distribution. Fig. 10 illustrates the 2D temperature distributions at $t = 10$ s for the tissue heated by an incident Gaussian heat flux $q_p = q_{p\max} \exp(-r^2/r_p^2)$, where $q_{p\max} = 4$ W/cm^2 and $r_p = 1$ cm for the surface heating (Fig. 10(a)) and $q_{p\max} = 150$ W/cm^2 and $r_p = 2$ cm for the body heating (Fig. 10(b)). For the latter, the Beer's law is used again to describe the volumetric heat source distribution in the axial di-

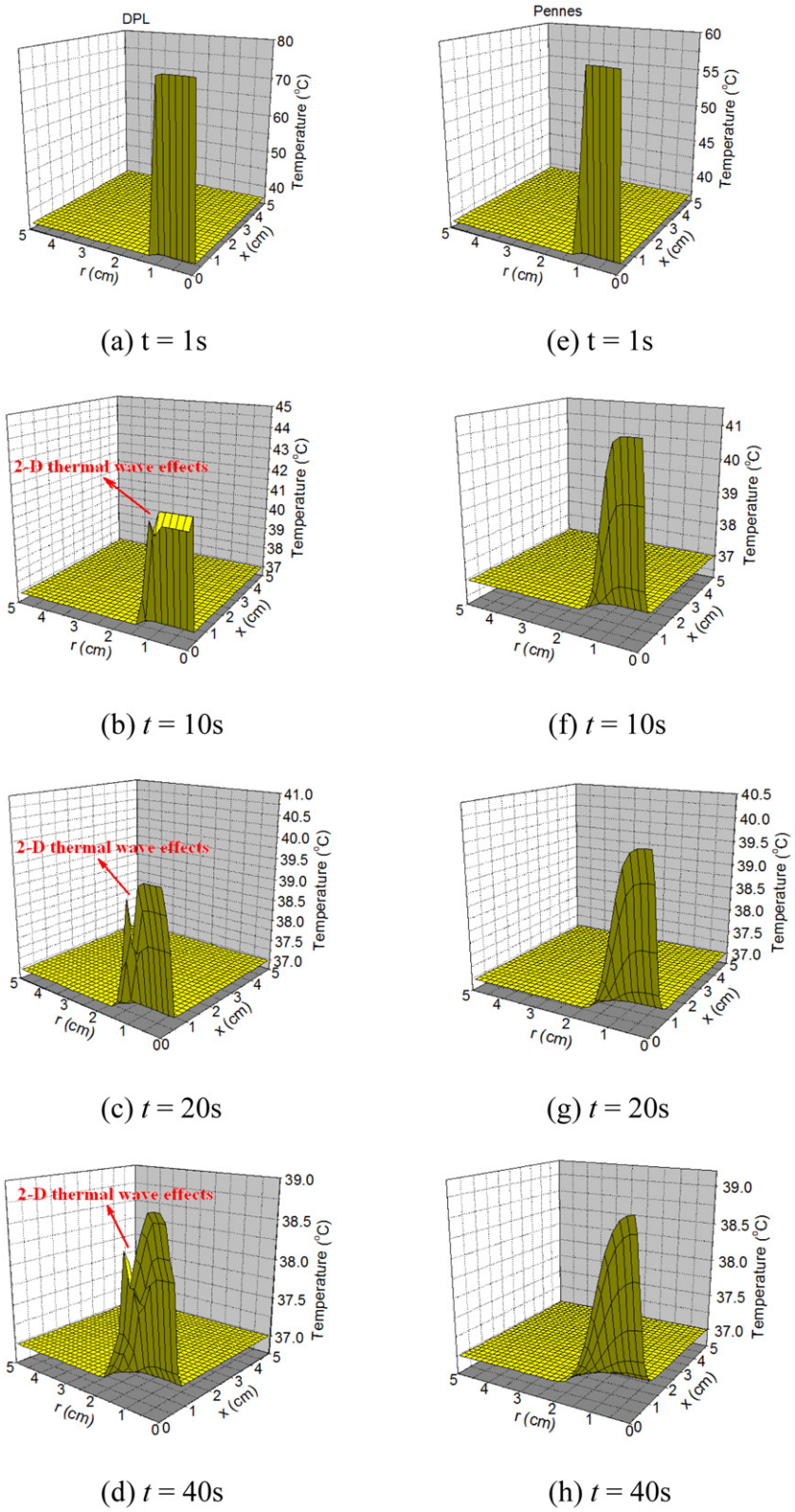

Fig. 7. 2D temperature distributions at different time instants. (a)–(d) DPL model; (e)–(f) Pennes model.

rection. The two lagging times used are $\tau_q = 8$ s and $\tau_T = 0.5$ s. As shown in Fig. 10, no thermal wave exhibits in the body heating case but in the surface heating case. Due to the non-uniform distribution of the incident heat flux, the 2D effect on the temperature transient is pronounced for both cases.

5. Conclusions

The DPL bioheat conduction equations in a 2D axisymmetric living tissue are derived for thermal transport in living biological tissues that incorporates the blood perfusion, metabolism and

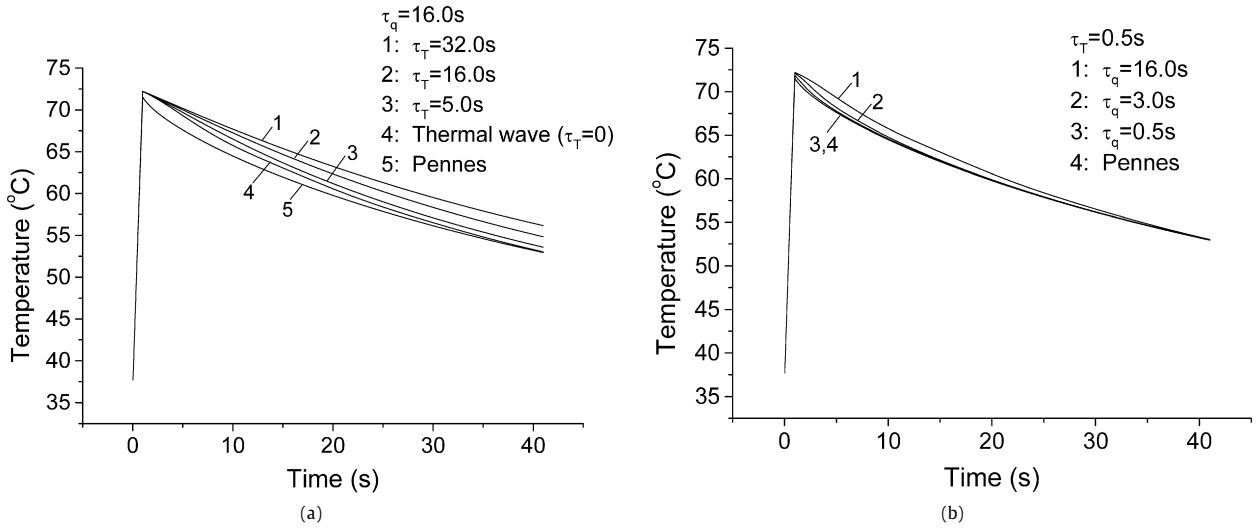

Fig. 8. Temperature transients at the point $(0, 0)$ for different combinations of τ_T and τ_q. (a) Influence of τ_T while τ_q keeps unchanged; (b) influence of τ_q while τ_T keeps unchanged.

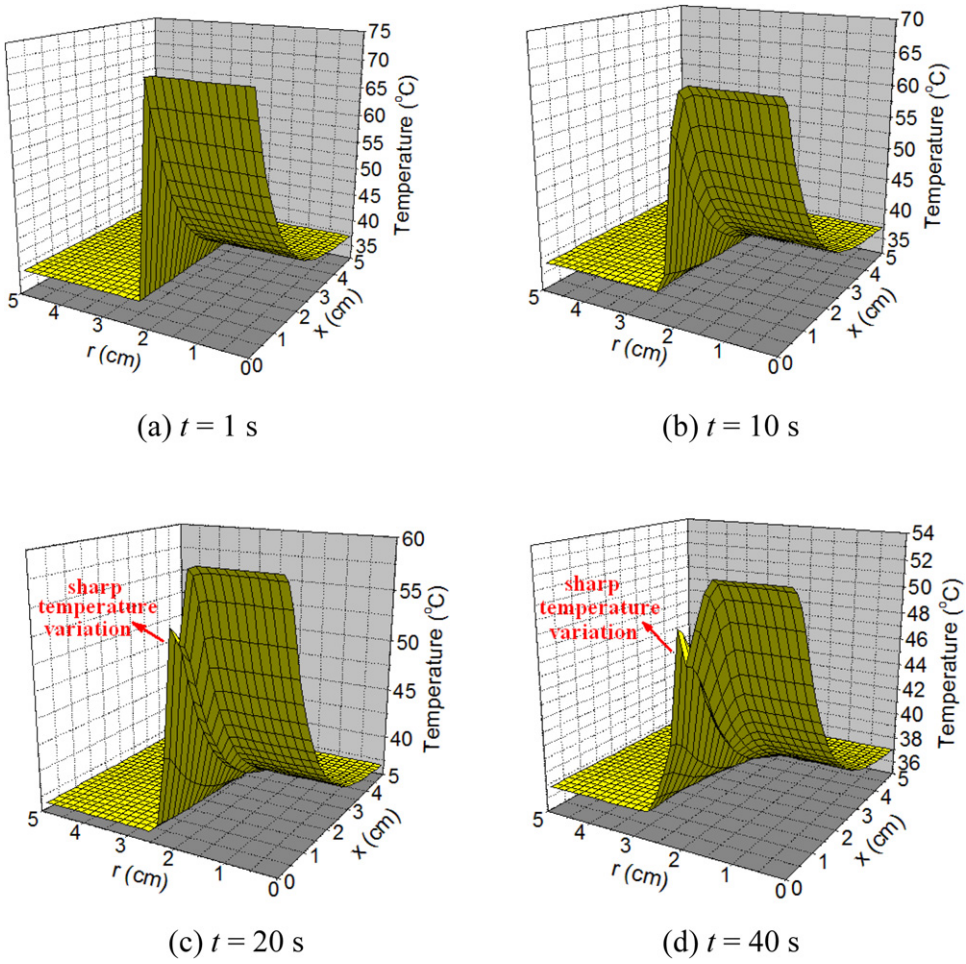

Fig. 9. 2D temperature distributions at different time instants for body heating. (a) $t = 1$ s; (b) $t = 10$ s; (c) $t = 20$ s; (d) $t = 40$ s.

other volumetric heat generations. Two local heating conditions, surface heating and body heating, are examined. The effects of the two phase lag times τ_T and τ_q on temperature transients are investigated. The numerical results show that the DPL bioheat conduction model describes different thermal responses from the thermal-wave and classical Pennes' bioheat models, depending on the values of the two lagging times. Due to the presence of the blood perfusion in living tissues, the DPL bioheat conduction model can reduce to the Pennes' bioheat conduction model only when $\tau_q = \tau_T = 0$. This is in contrast to the traditional DPL heat conduction model for which the condition $\tau_q = \tau_T$ (not necessarily equal to zero) is sufficient for it to reduce to the Fourier heat conduction model. The thermal wave effect is diminished as the lagging time τ_T increases. An over-diffusion could occur when τ_T

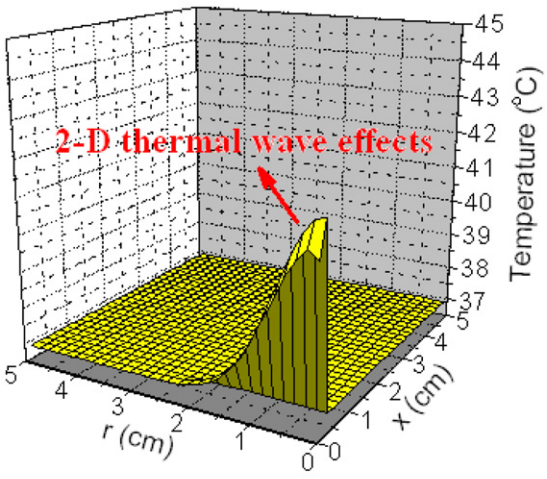

(a) Surface heating

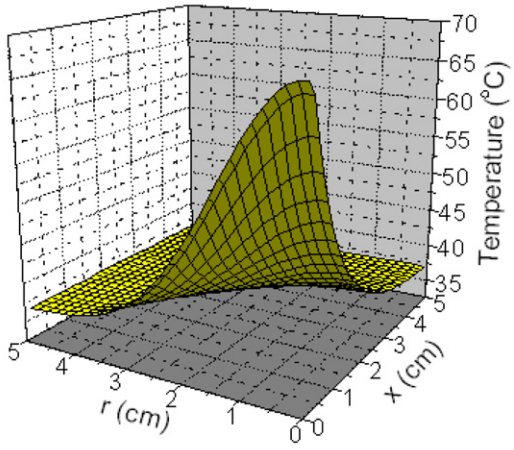

(b) Body heating

Fig. 10. 2D temperature distributions in the tissue heated by an incident Gaussian heat flux at $t = 10$ s. (a) Surface heating and (b) body heating.

is larger than τ_q. For local surface heating with a uniform incident heat flux, thermal wave exhibits in both the axial and radial directions, while it could only exhibit in the radial direction for a body heating. When the spot of a local heating is smaller than the tissue bulk size, the 2D effect may become pronounced, particularly for the region near the spot edge.

Appendix A

The control volume method [18] is employed to solve the governing equations (7) and (8) together with the initial and boundary conditions (9)–(11). The entire computational zone is divided into $L_x \times M_r$ control volumes. Each control volume is represented by a grid point placed at its geometric center. For example, the shadowed part shown in Fig. 2 represents a control volume P with faces e, w, n and s connecting to its neighbor control volumes E, W, N and S, respectively. The lengths of the control volume are Δx in the x-direction and Δr in the r-direction. The distances between two neighboring grid points in the x-direction are $(\delta x)_w$ and $(\delta x)_e$, and those in the r-direction are $(\delta r)_n$ and $(\delta r)_s$. In general, $(\delta x)_w \neq (\delta x)_e$ and $(\delta r)_n \neq (\delta r)_s$.

Integrating Eq. (7) over a control volume with the grid point P, for example, and over the time step from t to $t + \Delta t$ and then discretizing the result based on the backward difference in time and the piecewise-linear profile in space yields [18]:

$$a_P q_r|_P^{t+\Delta t} = a_N q_r|_N^{t+\Delta t} + a_S q_r|_S^{t+\Delta t} + b_r \tag{A.1}$$

where

$$a_N = \left(\frac{0.5\Delta x}{r_n} + \frac{\Delta x}{(\delta r)_n}\right)(\Delta t + \tau_T) \tag{A.2}$$

$$a_S = \left(-\frac{0.5\Delta x}{r_s} + \frac{\Delta x}{(\delta r)_s}\right)(\Delta t + \tau_T) \tag{A.3}$$

$$a_P = \frac{\Delta x \Delta r}{\alpha}\left(1 + \frac{\tau_q}{\Delta t}\right) - \frac{0.5\Delta x}{r_n}(\Delta t + \tau_T) + \frac{\Delta x}{(\delta r)_n}(\Delta t + \tau_T) + \frac{0.5\Delta x}{r_s}(\Delta t + \tau_T) + \frac{\Delta x}{(\delta r)_s}(\Delta t + \tau_T) \tag{A.4}$$

$$\begin{aligned} b_r = {} & \frac{\Delta x \Delta r}{\alpha}\left(q_r|_P^t + 2\frac{\tau_q}{\Delta t} q_r|_P^t - \frac{\tau_q}{\Delta t} q_r|_P^{t-\Delta t}\right) \\ & + 0.25(\Delta t + \tau_T)\left(q_x|_{NE}^{t+\Delta t} - q_x|_{SE}^{t+\Delta t} - q_x|_{NW}^{t+\Delta t} + q_x|_{SW}^{t+\Delta t}\right) \\ & - 0.25\tau_T\left(q_x|_{NE}^t - q_x|_{SE}^t - q_x|_{NW}^t + q_x|_{SW}^t\right) \\ & - 0.5\tau_T \Delta x\left(\frac{q_r|_N^t + q_r|_P^t}{r_n} - \frac{q_r|_S^t + q_r|_P^t}{r_s}\right) \\ & - \tau_T \Delta x\left(\frac{q_r|_N^t - q_r|_P^t}{(\delta r)_n} - \frac{q_r|_P^t - q_r|_S^t}{(\delta r)_s}\right) \\ & + 0.5 w_b \rho_b c_b \Delta x(\Delta t + \tau_T)\left(T|_N^{t+\Delta t} - T|_S^{t+\Delta t}\right) \\ & - 0.5\tau_T w_b \rho_b c_b \Delta x\left(T|_N^t - T|_S^t\right) \end{aligned} \tag{A.5}$$

In Eqs. (A.1) and (A.5), the symbols $q_i|_\xi^\zeta$ represents the heat flux component q_i $(i = x, r)$ at grid point ξ $(= P, E, W, N, S, NE, NW, SE, SW)$ at the time step ζ $(= t - \Delta t, t, t + \Delta t)$; $T|_\xi^\zeta$ represents the temperature at grid point ξ $(= N, S)$ at the time step ζ $(= t, t + \Delta t)$; r_n and r_s are the radii of the interfaces n and s, respectively.

Similarly, the equation governing the heat flux component in the x-direction can be discretized as follows:

$$a_P q_x|_P^{t+\Delta t} = a_E q_x|_E^{t+\Delta t} + a_W q_x|_W^{t+\Delta t}| + b_x \tag{A.6}$$

where

$$a_E = \frac{\Delta r}{(\delta x)_e}(\Delta t + \tau_T) \tag{A.7}$$

$$a_W = \frac{\Delta r}{(\delta x)_w}(\Delta t + \tau_T) \tag{A.8}$$

$$a_P = a_E + a_W + \frac{\Delta x \Delta r}{\alpha}\left(1 + \frac{\tau_q}{\Delta t}\right) \tag{A.9}$$

$$\begin{aligned} b_x = {} & \frac{\Delta x \Delta r}{\alpha}\left(q_z|_P^t + 2\frac{\tau_q}{\Delta t} q_x|_P^t - \frac{\tau_q}{\Delta t} q_x|_P^{t-\Delta t}\right) \\ & + 0.25(\Delta t + \tau_T)\left(q_r|_{NE}^{t+\Delta t} - q_r|_{SE}^{t+\Delta t} - q_r|_{NW}^{t+\Delta t} + q_r|_{SW}^{t+\Delta t}\right) \\ & - 0.25\tau_T\left(q_r|_{NE}^t - q_r|_{SE}^t - q_r|_{NW}^t + q_r|_{SW}^t\right) \\ & + 0.5\Delta r(\Delta t + \tau_T)\left(q_r|_E^{t+\Delta t} - q_r|_W^{t+\Delta t}\right)/r_P \\ & - 0.5\tau_T \Delta r\left(q_r|_E^t - q_r|_W^t\right)/r_P \\ & - 0.5\tau_T \Delta x\left(q_r|_N^t + q_r|_P^t\right)/r_n + 0.5\tau_T \Delta x\left(q_r|_S^t + q_r|_P^t\right)/r_s \\ & - \tau_T \Delta r\left(q_x|_E^t - q_x|_P^t\right)/(\delta x)_e + \tau_T \Delta r\left(q_x|_P^t - q_x|_W^t\right)/(\delta x)_w \\ & + 0.5 w_b \rho_b c_b \Delta x(\Delta t + \tau_T)\left(T|_E^{t+\Delta t} - T|_W^{t+\Delta t}\right) \\ & - 0.5\tau_T w_b \rho_b c_b \Delta x\left(T|_E^t - T|_W^t\right) \end{aligned} \tag{A.10}$$

The temperatures T in Eqs. (A.5) and (A.10) can be approximated by discretizing the bioheat energy equation (4). For example, the temperature at the grid point P is

$$T_P^{t+\Delta t} = \frac{1}{\rho c\Delta x\Delta r + w_b\rho_b c_b\Delta t\Delta x\Delta r} \times \left\{-0.5\Delta t\Delta x\left[r_n\left(q_r|_N^{t+\Delta t} + q_r|_P^{t+\Delta t}\right) - r_s\left(q_r|_P^{t+\Delta t} + q_r|_S^{t+\Delta t}\right)\right]/r_P - 0.5\Delta t\Delta r\left(q_x|_E^{t+\Delta t} - q_x|_W^{t+\Delta t}\right) + \Delta t\Delta x\Delta r Q_m + \Delta t\Delta x\Delta r w_b\rho_b c_b T_b + \rho c\Delta x\Delta r T_P^t\right\} \quad (A.11)$$

The discretized equation for the boundary grid points can be obtained in a similar way by following the general procedures described in Ref. [18]. The results will not be given here for brevity.

Eqs. (A.1), (A.6) and (A.11) involve quantities at three time instants, $t+\Delta t$, t, and $t-\Delta t$. Among them, the heat flux components and temperatures at the current time step $t+\Delta t$ need to be advanced. For convenience, Eq. (A.1) has been derived by grouping all the terms into b_r except for those involving $q_r|_P^{t+\Delta t}$, $q_r|_N^{t+\Delta t}$ and $q_r|_S^{t+\Delta t}$, and so has Eq. (A.6) in a similar way. With this treatment, they can easily be solved using the tri-diagonal matrix algorithm (TDMA). Since the term b_r in Eq. (A.1) and b_x in Eq. (A.6) both include several unknown heat flux components q_r and q_x and temperatures T at $t+\Delta t$ for each time step, an iterative solution will be conducted until a tolerance for convergence of the T values is met.

References

[1] H.H. Pennes, Analysis of tissue and arterial blood temperatures in the resting forearm, Journal of Applied Physiology 1 (1948) 93–122.

[2] J.S. Rastegar, Hyperbolic heat conduction in pulsed laser irradiation of tissue, in: M.J. Berry, G.M. Harpole (Eds.), Thermal and Optical Interactions with Biological and Related Composite Materials, Proceedings of the SPIE, vol. 1064, SPIE Press, Bellingham, WA, 1989, pp. 114–117.

[3] W. Kaminski, Hyperbolic heat conduction equation for materials with a nonhomogeneous inner structure, ASME Journal of Heat Transfer 112 (1990) 555–560.

[4] K. Mitra, S. Kumar, A. Vedavarz, M.K. Moallemi, Experimental evidence of hyperbolic heat conduction in processed meat, ASME Journal of Heat Transfer 117 (1995) 568–573.

[5] J. Liu, X. Chen, L.X. Xu, New thermal wave aspects on burn evaluation of skin subjected to instantaneous heating, IEEE Transactions on Biomedical Engineering 46 (1999) 420–428.

[6] T.C. Shih, H.S. Kou, C.T. Liauh, W.L. Lin, The impact of thermal wave characteristics on thermal dose distribution during thermal therapy: A numerical study, Medical Physics 32 (2005) 3029–3036.

[7] A. Banerjee, A.A. Ogale, C. Das, K. Mitra, C. Subramanian, Temperature distribution in different materials due to short pulse laser irradiation, Heat Transfer Engineering 26 (2005) 41–49.

[8] K. Kim, Z. Guo, Multi-time-scale heat transfer modeling of turbid tissues exposed to short-pulsed irradiations, Computer Methods and Programs in Biomedicine 86 (2007) 112–123.

[9] Y. Bayazitoglu, G.P. Peterson, Fundamental issues in hyperbolic heat conduction, in: ASME HTD, 1992, p. 227.

[10] C. Bai, A.S. Lavine, On the hyperbolic heat conduction and the second law of thermodynamics, ASME Journal of Heat Transfer 117 (1995) 256–263.

[11] C. Korner, H.W. Bergmann, The physical defects of the hyperbolic heat conduction equation, Applied Physics A 67 (1998) 397–401.

[12] P.J. Antaki, New interpretation of non-Fourier heat conduction in processed meat, ASME Journal of Heat Transfer 127 (2005) 189–193.

[13] D.Y. Tzou, A unified field approach for heat conduction from macro- to microscales, ASME Journal of Heat Transfer 117 (1995) 8–16.

[14] F. Xu, T.J. Lu, K.A. Seffen, Biothermomechanical behavior of skin tissue, Acta Mech. Sin. 24 (2008) 1–23.

[15] B. Shen, P. Zhang, Notable physical anomalies manifested in non-Fourier heat conduction under the dual-phase-lag model, International Journal of Heat and Mass Transfer 51 (2008) 1713–1727.

[16] J. Zhou, J.K. Chen, Y. Zhang, Dual-phase-lag effects on thermal damage to biological tissues caused by laser irradiations, Computers in Biology and Medicine (2009), in press.

[17] F. Xu, K.A. Seffen, T.J. Liu, Non-Fourier analysis of skin biothermomechanics, International Journal of Heat and Mass Transfer 51 (2008) 2237–2259.

[18] S.V. Patankar, Numerical Heat Transfer and Fluid Flow, Hemisphere Publishing Corp., New York, 1980.

[19] Y. Yamada, T. Tien, M. Ohta, Theoretical analysis of temperature variation of biological tissues irradiated by light, in: L.S. Fletcher, T. Aihara (Eds.), Proceedings of the ASME/JSME Joint Thermal Engineering Conference, vol. 4, Amazon, Maui, Hawaii, 1995, pp. 575–581.

[20] D.W. Tang, N. Araki, Non-Fourier heat conduction behavior in finite mediums under pulse surface heating, Materials Science and Engineering A 292 (2000) 173–178.